

Mars Exploration Rover Airbag Landing Loads Testing and Analysis

Douglas S. Adams*
Jet Propulsion Laboratory, Pasadena, CA, 91109

This paper presents a summary of the testing and analysis used to quantify the expected airbag landing loads for the Mars Exploration Rovers. The airbag drop test setup, lander instrumentation, and the test data reduction method are discussed in order to provide an understanding of the empirical loads. A set of limiting cases that bound the empirical data are developed for use in finite element modeling of the lander and rover models. A favorable comparison is made between the empirical data and available computational airbag models boosting confidence in the results.

Nomenclature

$\vec{\alpha}$	= angular acceleration vector of the lander
\vec{a}_c	= acceleration vector of the accelerometer pattern center point C
\vec{a}_G	= acceleration vector of the lander center of gravity G
$\vec{a}_{P,Q,R,S}$	= acceleration vector of the individual triaxial accelerometers P , Q , R , and S
$\ a\ _{\max}$	= maximum acceleration magnitude at a given distance from the center of gravity for planar motion
C	= center point of the accelerometer pattern
A_{calc}	= column vector of the calculated body frame acceleration terms
A_{meas}	= column vector of the measured body frame accelerations
K	= matrix containing rigid body translation between C and the individual accelerometers P , Q , R , and S
\tilde{K}	= right half of the K matrix
LUF	= load uncertainty factor
P, Q, R, S	= locations of the triaxial accelerometer blocks
$\vec{r}_{C/G}$	= position vector of the accelerometer pattern center point C with respect to the center of gravity G
$\vec{r}_{P,Q,R,S/C}$	= position vector of P , Q , R , and S , with respect to the accelerometer pattern center point C
\vec{v}_c	= velocity vector of the accelerometer pattern center point C
$\vec{v}_{P,Q,R,S}$	= velocity vector of P , Q , R , and S , determined by integrating body frame accelerations
V_{calc}	= column vector of the sensing point velocities and angular rates calculated from V_{meas}
V_{meas}	= column vector of the sensing point velocities determined by integrating body frame accelerations
$\vec{\omega}$	= angular rate vector of the lander
W	= left half of the K matrix, also the rigid body velocity transformation between C and P , Q , R , and S

I. Introduction

THE Mars Exploration Rover (MER) airbag system employed in the twin Spirit and Opportunity landings is designed to provide high survivability for the rover payload in areas that would otherwise be difficult to attempt. The MER airbags are geometrically the same as the ones used on the successful 1997 Mars Pathfinder mission^{1,2} but have been strengthened to accommodate the more than 40% increase in lander mass (from 290 kg to 415 kg) for MER; the total MER landed mass including airbags was 540 kg. While the mass of the airbags is

* Staff Engineer, Spacecraft Structures and Dynamics Group, Jet Propulsion Laboratory, MS: 157-410, 4800 Oak Grove Dr., Pasadena, CA, 91109, AIAA Member.

comparable to a propulsion system, the landing loads are high and must be considered omnidirectional as an impact event could occur at any orientation.

The operation and durability of the airbags was evaluated in a series of 52 drop tests done at Mars atmospheric pressure under flight like velocities and incident angles. The primary objective of these tests was to determine the airbag failure modes and any weakness in the system by observing the interaction of the airbags with the impact zone using high-speed cameras and through post-test damage inspection. The design was then iterated between test series in order to mitigate as many of the failure modes as possible. In addition to ensuring the survival of the airbags, a second objective of the tests was to experimentally measure the loads on the lander and to detect any "stroke-out" failures. A stroke-out can occur in a high energy impact if the lander strikes a rock through the airbag. This would not necessarily damage the airbag but could result in catastrophic damage to the lander.

There are several different types of landing loads that were measured during the course of the drop tests. The first, and most obvious, is the peak linear acceleration magnitude sensed during an impact. The second is the angular acceleration α and the angular rate ω accompanying the linear acceleration in an oblique impact with the surface. The third is a measurement of the tendon pin loads; the tendon pins are the attachment points for the Kevlar and Vectran airbag tendons that hold the airbags in place on the lander petals. The tendon pin loads proved to be the most problematic both to measure and to simulate and are not included in the present discussion. Finally, although it's not strictly a load, as mentioned before the lander stroke was also an important quantity as it has direct bearing on the airbag system's capabilities.

This paper reviews the test instrumentation, the data analysis technique, and the final results obtained from the 52 MER vacuum chamber drop tests. A stochastic approach is then used to determine the MER design loads based on the test results and is shown to bound the expected loads. Finally, analysis tools and models used to estimate the landing loads are briefly discussed and a comparison of the predicted and measured loads is made.

II. Drop Test Facilities and Setup and Lander Instrumentation

The airbag drop tests were performed in the Space Power Facility (SPF) vacuum chamber at NASA's Plum Brook Station in Sandusky, Ohio. This facility is home to the world's largest vacuum chamber with a working diameter of 100 ft and a dome height of 122 ft. The drop test setup in the SPF vacuum chamber is illustrated schematically in Fig. 1. The test lander, complete with airbags and an onboard data system, was suspended from the roof of the SPF chamber above a ramp inclined at angles of 0, 45, 60, and 72 degrees from the horizontal. The target section of the ramp was populated with volcanic rocks ranging in size from 0.1 to 0.5 m in height in order to simulate a more realistic (if not severe) impact zone. These rocks were believed to be representative of the different sizes present at the chosen landing sites in the Gusev Crater and on the Meridiani Planum.

After the chamber pressure reached a level of 4 torr, the airbags were inflated to 1.0 psia (some alternate pressures were also tested) using a nitrogen umbilical and then released. A bungee system was used to augment the gravitational acceleration of the test article in order to achieve impact velocities as high as 25 m/s (56 mph). A cable cutter was used to release the lander immediately prior to impact resulting in a brief freefall and accurate free body impact dynamics. Following the primary impact the lander's motion was arrested by the catch net with the lander coming to rest on a foam padded area below the ramp.

The test lander, shown in Fig. 2, was constructed from an aluminum frame and included steel weights to approximate the mass and inertia properties of the flight hardware. The interior was hollow with a 0.25 in aluminum plate across the base petal on which all of the instrumentation was mounted with the exception of the load cells. The steel ballast weights for petals 1 and 3

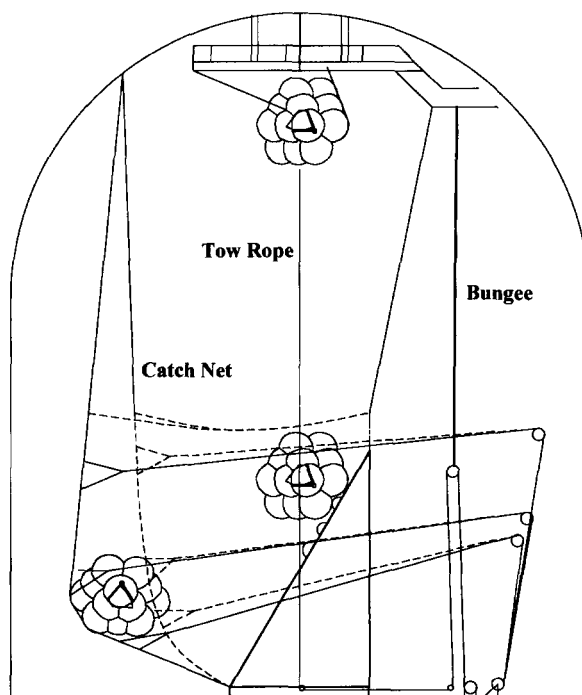


Figure 1: Profile view of the MER drop test configuration in the SPF vacuum chamber³.

are visible in Fig. 2 bolted to the aluminum petal structure. Petal 4 is the base petal and petal 2 is folded down in this view. Also visible in Fig. 2 are the accelerometers, which are mounted in a cruciform pattern that is oriented slightly counterclockwise and can be identified by the small protective white foam blocks covering them. This test also included a fifth accelerometer block mounted at the center of the base plate. The foam blocks are used to shield the accelerometers from contact with the white airbag inflation hoses during the impact event.

The data for each test was collected by the onboard IDDAS system, which recorded up to 39 channels of data. Some tests also included a second IDDAS unit with an additional 24 channels for a total capability of 63 channels. The single 39-channel IDDAS unit is visible in the lower right of Fig. 2 with its power supply in the lower left.



Figure 2: The test lander interior in the configuration used for the final test series.

During the course of the testing series there were as many as 55 onboard data channels that were recorded at a 2000 Hz sample rate. The primary data channels carried on every test were the four airbag pressures, the chamber pressure, and a set of 4 triaxial accelerometers (12 channels). Auxiliary data channels that were used on some of the tests include rate gyros, additional accelerometers, tendon pin load cells, string pots for measuring stroke, and straininserted lander petal latch pins. Each of these data channels was used to evaluate one or more aspect of the airbag performance under given test conditions, which were also varied in order to simulate a range of impact severities. With the exception of the rate gyros, most of the auxiliary sensors were only carried on a small number of the earlier tests.

III. Accelerometer Data Analysis

Because rate gyros were not always available for a given test it was necessary to evaluate the angular acceleration and rate terms using the available accelerometer data. In order to simplify this process the triaxial accelerometers were arranged in a symmetric pattern about a central point on the base plate of the lander. The accelerometers were originally mounted in a cruciform pattern as shown in Fig. 3a. The cruciform pattern had the advantage of providing redundant checks for the acceleration at the center point “C” as

$$\bar{a}_C = (\bar{a}_P + \bar{a}_Q) / 2 = (\bar{a}_R + \bar{a}_S) / 2 \quad (1)$$

Later, due to additional equipment requirements, the accelerometers were moved to an equilateral triangle pattern, shown in Fig. 3b, where a fourth accelerometer was positioned at the center of the circle described by P, Q, and R. Again, this served as a redundant check for the acceleration measurements as

$$\bar{a}_C = \bar{a}_S = (\bar{a}_P + \bar{a}_Q + \bar{a}_R) / 3 \quad (2)$$

In fact, in general, the acceleration at the center of a planar circle fixed in a rigid body is identically equal to the average acceleration of 2 or more equally spaced accelerometers with their axes aligned lying on the circle due to the symmetry of the measurements; even numbers are better as they provide more verification opportunities.

The minimum number of triaxial accelerometers required to describe the full six degree-of-freedom motion of a rigid body is three. Of course, the minimum number of single axis accelerometers is six; however, due to the collocation of accelerometers configured in triaxial blocks the minimum number of channels increases to nine for three

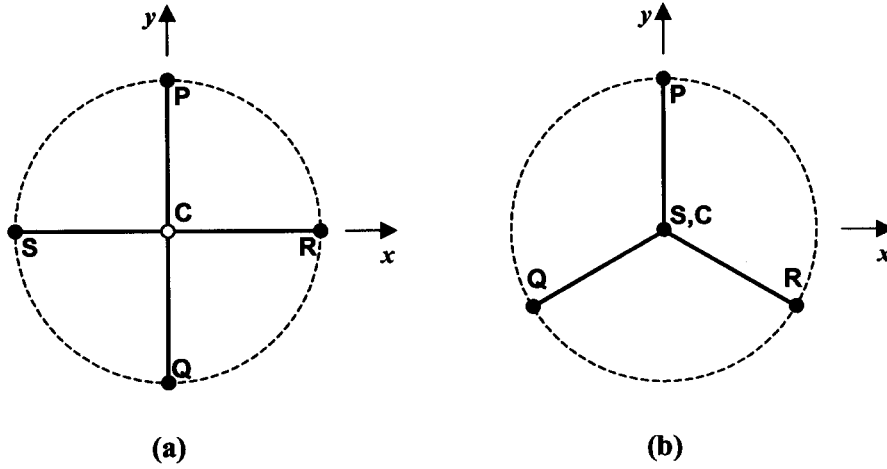


Figure 3: (a) Cruciform accelerometer pattern used on the majority of tests. (b) Triangular accelerometer pattern with redundant central measurement used on tests having special equipment requirements.

blocks arranged in non-colinear positions. In practice, the redundancy in measurements was welcomed in the test and provided a means of averaging the results and of crosschecking them against each other.

Assuming that the test lander behaves as a rigid body we can express the accelerations at the sensing locations in body frame (lander) coordinates³ in vector form as

$$\vec{a}_P = \vec{a}_C + \vec{\alpha} \times \vec{r}_{P/C} + \vec{\omega} \times \vec{\omega} \times \vec{r}_{P/C} \quad (3)$$

$$\vec{a}_Q = \vec{a}_C + \vec{\alpha} \times \vec{r}_{Q/C} + \vec{\omega} \times \vec{\omega} \times \vec{r}_{Q/C} \quad (4)$$

$$\vec{a}_R = \vec{a}_C + \vec{\alpha} \times \vec{r}_{R/C} + \vec{\omega} \times \vec{\omega} \times \vec{r}_{R/C} \quad (5)$$

$$\vec{a}_S = \vec{a}_C + \vec{\alpha} \times \vec{r}_{S/C} + \vec{\omega} \times \vec{\omega} \times \vec{r}_{S/C} \quad (6)$$

or in expanded form as

$$\begin{bmatrix} a_{Px} \\ a_{Py} \\ a_{Pz} \\ a_{Qx} \\ a_{Qy} \\ a_{Qz} \\ a_{Rx} \\ a_{Ry} \\ a_{Rz} \\ a_{Sx} \\ a_{Sy} \\ a_{Sz} \end{bmatrix} = \begin{bmatrix} 1 & 0 & 0 & 0 & r_{Pz} & -r_{Py} & 0 & -r_{Px} & -r_{Px} & r_{Py} & r_{Pz} & 0 \\ 0 & 1 & 0 & -r_{Pz} & 0 & r_{Px} & -r_{Py} & 0 & -r_{Py} & r_{Px} & 0 & r_{Pz} \\ 0 & 0 & 1 & r_{Py} & -r_{Px} & 0 & -r_{Pz} & -r_{Pz} & 0 & 0 & r_{Px} & r_{Py} \\ 1 & 0 & 0 & 0 & r_{Qz} & -r_{Qy} & 0 & -r_{Qx} & -r_{Qx} & r_{Qy} & r_{Qz} & 0 \\ 0 & 1 & 0 & -r_{Qz} & 0 & r_{Qx} & -r_{Qy} & 0 & -r_{Qy} & r_{Qx} & 0 & r_{Qz} \\ 0 & 0 & 1 & r_{Qy} & -r_{Qx} & 0 & -r_{Qz} & -r_{Qz} & 0 & 0 & r_{Qx} & r_{Qy} \\ 1 & 0 & 0 & 0 & r_{Rz} & -r_{Ry} & 0 & -r_{Rx} & -r_{Rx} & r_{Ry} & r_{Rz} & 0 \\ 0 & 1 & 0 & -r_{Rz} & 0 & r_{Rx} & -r_{Ry} & 0 & -r_{Ry} & r_{Rx} & 0 & r_{Rz} \\ 0 & 0 & 1 & r_{Ry} & -r_{Rx} & 0 & -r_{Rz} & -r_{Rz} & 0 & 0 & r_{Rx} & r_{Ry} \\ 1 & 0 & 0 & 0 & r_{Sx} & -r_{Sy} & 0 & -r_{Sx} & -r_{Sx} & r_{Sy} & r_{Sx} & 0 \\ 0 & 1 & 0 & -r_{Sx} & 0 & r_{Sx} & -r_{Sy} & 0 & -r_{Sy} & r_{Sx} & 0 & r_{Sx} \\ 0 & 0 & 1 & r_{Sy} & -r_{Sx} & 0 & -r_{Sx} & -r_{Sx} & 0 & 0 & r_{Sx} & r_{Sy} \end{bmatrix} \begin{bmatrix} a_{Cx} \\ a_{Cy} \\ a_{Cz} \\ \alpha_x \\ \alpha_y \\ \alpha_z \\ \omega_x^2 \\ \omega_y^2 \\ \omega_z^2 \\ \omega_x \omega_y \\ \omega_x \omega_z \\ \omega_y \omega_z \end{bmatrix} \quad (7)$$

where the position vectors are relative to the accelerometer array center point "C". Equation 7 is more conveniently expressed in matrix form as

$$A_{meas} = KA_{calc} \quad (8)$$

where the left hand side represents the measured accelerations in the body frame and the right hand side is the calculated rigid body expression relating the sensing point accelerations to the rigid body motion. In the planar configuration used for the drop tests the r_z terms are zero, which simplifies the K matrix somewhat. Later it will be useful to think of the K matrix as being formed of two 12x6 submatrices as

$$[K] = [W \tilde{K}] \quad (9)$$

The issue that arises is that, regardless of the number of accelerometers employed, the K matrix will always have a rank of 9 while there are actually 12 unknowns. The rank deficiency of K is due to the presence of the ω cross product terms, which requires the determination of the ω values prior to solving for the a_c and α values. To solve for the ω values we write the expression for the acceleration at a point in the body as observed from an inertial reference frame using the intermediate positions of the center of gravity “ G ” and the center of the accelerometer array “ C ”

$$\bar{a}_P = \bar{a}_G + \bar{\alpha} \times \bar{r}_{C/G} + \bar{\omega} \times \bar{\omega} \times \bar{r}_{C/G} + \bar{\alpha} \times \bar{r}_{P/C} + \bar{\omega} \times \bar{\omega} \times \bar{r}_{P/C} \quad (10)$$

If we integrate this expression, where all vectors are expressed in the body frame, then we find that all of the quantities referencing the center of gravity G and the array center C are uniform for all sensing points. Furthermore, the $\bar{\omega} \times \bar{\omega} \times \bar{r}_{P/C}$ terms always act perpendicularly to the acceleration due to $\bar{\alpha}_{P/C}$, thus, the velocities resulting from integrating the test measured accelerations, while meaningless due to the accelerated reference frame, are still useful in determining the angular rates provided that the integration starts at rest or with known angular rates. It is important to remove any DC error from the test data by subtracting the pre-drop signals and then adding the gravity vector back in to get correct sensing. This requires knowledge of the pre-drop orientation, which was difficult.

The velocities at the sensing points relative to the center point are expressed in the body frame as

$$\bar{v}_P = \bar{v}_C + \bar{\omega} \times \bar{r}_{P/C} \quad (11)$$

$$\bar{v}_Q = \bar{v}_C + \bar{\omega} \times \bar{r}_{Q/C} \quad (12)$$

$$\bar{v}_R = \bar{v}_C + \bar{\omega} \times \bar{r}_{R/C} \quad (13)$$

$$\bar{v}_S = \bar{v}_C + \bar{\omega} \times \bar{r}_{S/C} \quad (14)$$

or in matrix form as

$$V_{meas} = WV_{calc} \quad (15)$$

where the W matrix is the same as the left half of the K matrix identified in Eq. 9. The V_{meas} quantity is simply the result of the body frame integrated accelerations. The unknown $V_{calc} = [v_{Cx} \ v_{Cy} \ v_{Cz} \ \omega_x \ \omega_y \ \omega_z]^T$ values can then be solved for using a pseudo inverse of the W matrix, which has a rank of 6, giving the least squares result of

$$V_{calc} = [W^T W]^{-1} W^T V_{meas} \quad (16)$$

Having solved for the desired ω values (and ignoring the calculated velocities) we can then back substitute in order to determine the a_c and α terms. From Eqs. 8 and 9 we find the calculated acceleration quantities as

$$A_{calc} = [W^T W]^{-1} W^T \left[A_{meas} - \tilde{K} \begin{bmatrix} \omega^2 \\ \omega\omega \end{bmatrix} \right] \quad (17)$$

Knowing α , ω , and a_c we can then express the acceleration at the center of gravity as

$$\bar{a}_G = \bar{a}_C + \bar{\alpha} \times \bar{r}_{G/C} + \bar{\omega} \times \bar{\omega} \times \bar{r}_{G/C} \quad (18)$$

Here the center of gravity is assumed to be the instantaneous center of rotation for all of these operations. However, due to the deformable nature of the airbag system, the actual center of rotation is an unknown position that varies with time. Determination of the center of rotation would require a measurement of the forces acting on the airbag

due to its contact with the ramp. Since this measurement is not available it is assumed, for the purpose of this analysis, that the cg approximates the center of rotation and, unfortunately, even the cg was not known to a high precision.

Results from this analysis were verified by calculating the accelerations at the sensing points using the determined α , ω , and a_c values for the lander and comparing them to the test measured accelerations and angular rates as shown in Fig. 4 and Fig. 5 for Drop 15. As a general rule the acceleration reproductions were better than the ω reproductions; some of the ω discrepancies were attributed to small errors in the acceleration measurements, which have a larger affect on the angular rate determination.

Finally, the rotation is assumed to take place in a plane perpendicular to an axis through the center of gravity such that the maximum acceleration at any point in the body can be determined as

$$\|a\|_{\max} = \left(\|a_G\| + \sqrt{(\alpha r)^2 + (\omega^2 r)^2} \right)_{\max} \quad (19)$$

where the square root term is referred to as α_{pseudo} and represents the maximum possible acceleration component due to rotational terms for a given distance from the center of gravity⁴.

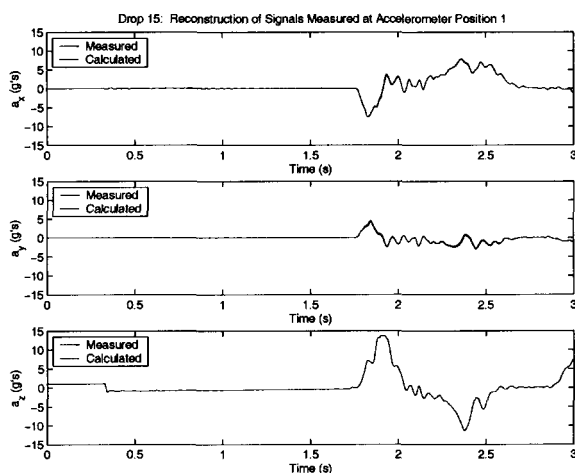


Figure 4. A comparison of measured and reconstructed accelerations at position 1 = P for Drop Test 15. These results indicate that the rigid body motion determined from the accelerometer signal analysis is accurate in reproducing the measured accelerations.

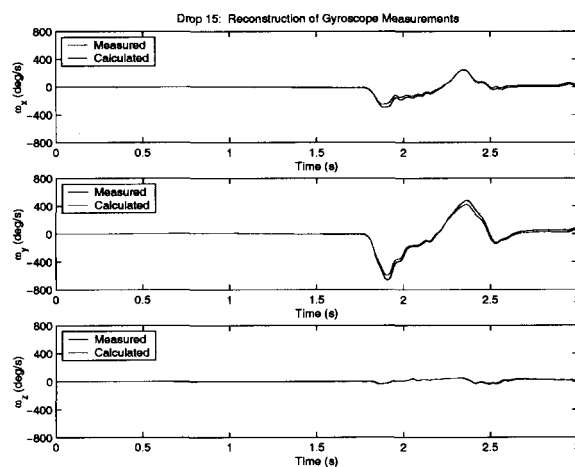


Figure 5. A comparison of gyroscope measured and the accelerometer determined angular rates for Drop Test 15. These results indicate that the rigid body motion determined from the accelerometer signal analysis is accurate in reproducing the measured angular rates and angular accelerations.

IV. Drop Test Results

A. Horizontal Ramp Results

One of the most important subsets of the drop test data is the series of four tests, Drops 33-36, done with a freefall impact of the lander (no bungee) on a 0° ramp⁵. These “superflat” tests have very small rotational terms and provide a baseline of unambiguous peak accelerations of the lander for a well-defined component of velocity normal to the surface. Data from these tests with no load uncertainty factor (LUF) is summarized in Table 1 and is fitted with a least squares line in Fig. 6. The line in Fig. 6 represents the minimum expected acceleration for all the drop tests as a function of the impact velocity normal to the ramp. The superflat tests are also important in

Table 1: Superflat (0° ramp) impact velocity and cg acceleration results.

Drop Number	Vnorm (m/s)	ag (g's)
33	11.4	14.7
34	11.9	15.8
35	15.1	22.7
36	16.3	25.1

helping to evaluate secondary impacts where the angular acceleration is likely to be small but the normal component may be higher than the nominal first impact maximum value of 12 m/s due to interaction with terrain features.

Using the linear fit of this data shown in Fig. 6 and extrapolating to a normal component of 16 m/s gives a cg acceleration with a 10% LUF of

$$|a_g|_{16m/s} = 1.1 * [(2.151 * 16 - 9.825) - 5/8] \quad (20)$$

$$|a_g|_{16m/s} = 26.4 \text{ g's} \quad (21)$$

where the difference between Earth and Mars gravity of 5/8 g's has been removed. This then represents the maximum secondary impact cg acceleration for a normal velocity of 16 m/s with a negligible angular acceleration component. A LUF of 1.10 is used for the high normal velocity case, which is intended to approximate the conditions potentially present in a secondary impact. This is slightly lower than the LUF of 1.15 used for an oblique impact because there is less uncertainty in the non-rotating impact acceleration and the peak acceleration normal to the surface should be similar for rotating secondary impacts having nearly constant rotation rates.

Unfortunately, there is some discrepancy in the velocity measurements for the superflat tests, which has some bearing on these results. Because these were free drops (no bungee was used) the only available measurements of velocity were from the radar gun and from integration of the onboard accelerometer data. These two approaches give slightly different results, which has a pronounced effect on the appearance of the data when plotted. The radar velocities are used in the present analysis, as they were a more direct measurement of the velocity.

B. Inclined Ramp Results

The peak cg accelerations for all inclined ramp drops having airbag inflation pressures and lander masses similar to the flight hardware are plotted along with the superflat data in Fig. 6. A key issue that arises is that of contending with the scatter in the data that is evident in Fig. 6. This scatter arises from uncertainty in the location of the center of rotation during the impact and from friction forces acting parallel to the ramp. Without additional information (e.g., the external force vector) the location of the center of rotation cannot be uniquely determined and thus it is impossible to know whether rotational components are included in the accelerations measured at the estimated cg

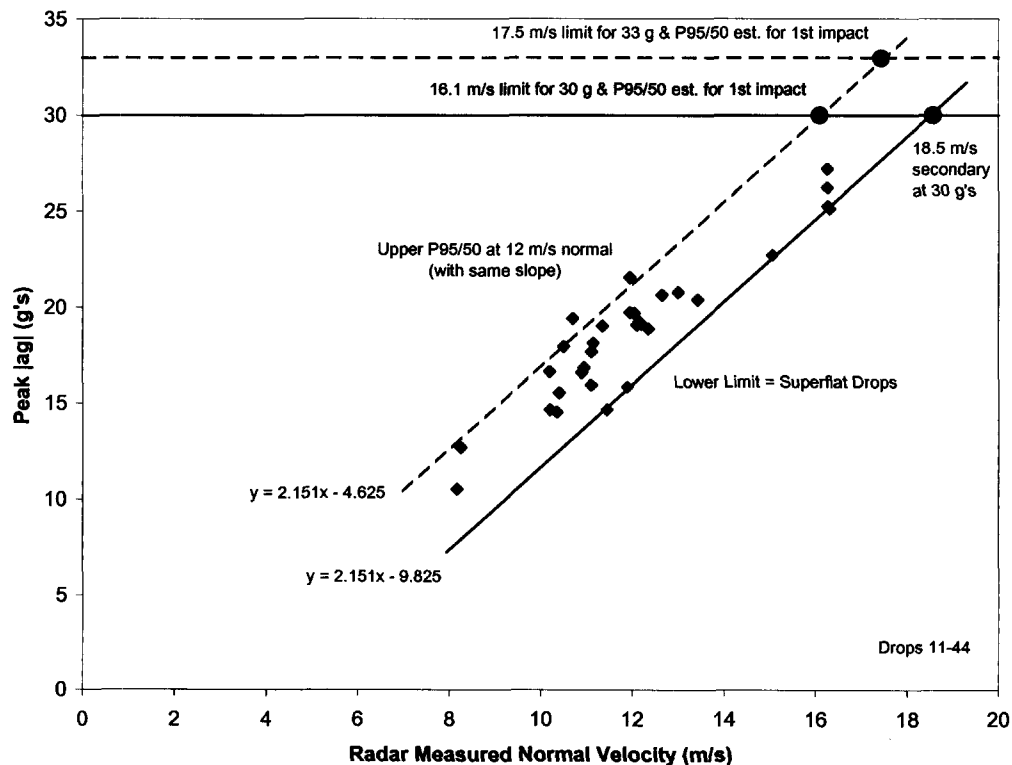


Figure 6: Summary of drop test peak cg accelerations as a function of normal velocity.

location. In fact, there will almost certainly be some rotational acceleration components that contribute to the scatter observed in the plotted data. Nevertheless, the estimated cg location does appear to be close to the center of rotation with the test results generally behaving as expected.

Since the primary interest here is in determining an upper bound for the anticipated worst-case accelerations, one approach is to restrict the normal component of velocity to a specific range and then to analyze the statistical behavior of the data that falls within that range. If we assume the data follows a normal distribution then we can calculate a P95/50 value for the maximum anticipated linear acceleration at the cg for the chosen subset of data. The P95/50 level is the level at which 95% of the population will be below that level with a 50% confidence⁶. The P95/50 level is calculated as

$$L_x = \bar{x} + k_n \sigma \tag{22}$$

where \bar{x} is the mean, σ is the standard deviation, and k_n is the normal tolerance factor (about 1.7 for n=10).

Nominally the maximum normal component of velocity for the first impact on Mars should be no higher than 12 m/s. Thus, restricting the normal velocity to a range of $11 < V_{norm} < 13$ m/s and removing the superflat cases from consideration gives the reduced data set in Table 2 which results in a P95/50 acceleration of 21.5 g's. If the normal velocity is restricted to a narrower range of $11.5 < V_{norm} < 12.5$ m/s as given in Table 3 then the P95/50 acceleration drops slightly to 21.2 g's. The reason for this is a decrease in the standard deviation while the mean value remains relatively constant. No attempt to correct for Mars gravity was made with the ramp drops due to the stochastic nature of the measured data.

C. Combined Linear and Angular Accelerations

One of the key features of the airbag data analysis was the determination of the angular rates and angular accelerations associated with an oblique impact. These angular terms determine the sensed accelerations at points in the lander and rover away from the cg where their contribution to the total acceleration can be high.

The data analysis results for Drop Test 15 on a 60° ramp are shown in Fig. 7. It is important to notice that, as indicated in Fig. 7, the peak acceleration may occur at different times for different distances from the cg due to the strong rotational component of the total acceleration. Also, the angular acceleration typically drops close to zero near the time of maxim cg acceleration, which coincides with the maximum airbag stroke (this is important for secondary impacts).

The most severe loads on the lander occur in the case where there is a high angular acceleration in combination with a high linear acceleration (angular rates were found not to be significant contributors to structural loads). This situation is most likely to occur during the first impact where the lander can potentially have a large horizontal velocity in addition to the normal component but with negligible angular rates. These conditions were simulated with the oblique ramp drops having normal velocities in the neighborhood of the design maximum normal component velocity of 12 m/s. Perhaps the simplest way of bounding these loads would be to combine the peak angular acceleration and linear acceleration into a single contrived event. However, we know from the test data that this is overly conservative as the angular acceleration typically peaks before the cg acceleration does. This is best illustrated by the phase diagram in Fig. 8,

Table 2: Results and statistical information for drops with a normal velocity component restricted to $11 < V_{norm} < 13$ m/s not including the superflat cases (no LUF).

11 m/s < Vnorm < 13 m/s			ag Statistics	
Drop Number	Vnorm (m/s)	ag (g's)	Max	21.5
15	11.1	17.7	Min	15.9
20	12.0	21.5	Mean	19.1
23	12.1	19.1	Sigma	1.4
24	11.1	15.9	P95/50	21.5
26	12.4	18.9		
26A	12.2	19.1		
27	12.0	19.7		
30	12.2	19.2		
31	12.1	19.7		
32	12.7	20.6		
38	11.2	18.1		
39	11.4	19.0		

Table 3: Results and statistical information for drops with a normal velocity component further restricted to $11.5 < V_{norm} < 12.5$ m/s not including the superflat cases (no LUF).

11.5 m/s < Vnorm < 12.5 m/s			ag Statistics	
Drop Number	Vnorm (m/s)	ag (g's)	Max	21.5
20	12.0	21.5	Min	18.9
23	12.1	19.1	Mean	19.6
26	12.4	18.9	Sigma	0.9
26A	12.2	19.1	P95/50	21.2
27	12.0	19.7		
30	12.2	19.2		
31	12.1	19.7		

which shows the magnitude of the angular acceleration α versus the cg acceleration for the drops listed in Table 3. From Fig. 8 it is apparent that a loading event that combines maximum angular acceleration with maximum linear acceleration would be well outside the observed phase plane envelope.

In order to make use of this data a set of characteristic worst-case events was developed in order to bound the observed data. This set of loading events was then used in the finite element analysis of the lander and rover in order to determine the internal loads in the structure⁷. Based largely on the phase plot in Fig. 8, and on the superflat and statistical ramp data from Fig. 6, a total of three characteristic load events were selected and are summarized in Table 4. Loading event 1 was selected to represent a typical high acceleration oblique impact and includes the test measured α and ω values. Loading event 2 was selected to represent a high α case where the simultaneous acceleration is also retained. Loading event 3 is intended to account for any secondary impacts that may have high normal acceleration but relatively low α as the lander would have already reached a nearly steady-state rotation rate following the first impact.

The heavy dashed line in Fig. 8 connects the 3 acceleration cases listed in Table 4 which are intended to characterize the three anticipated landing load extremes; these three points generally envelope the loads observed in the drop tests. The one case that falls outside these three points is Drop 20, which was the most severe of all the tests with the 60° ramp. The difference is minor, however, and Drop 20 could be classified as an outlier especially considering the consistency of the other data plotted in Fig. 8. Also, the post-impact cg acceleration DC error was unusually high for Drop 20 indicating that the peak level may be artificially high. This is

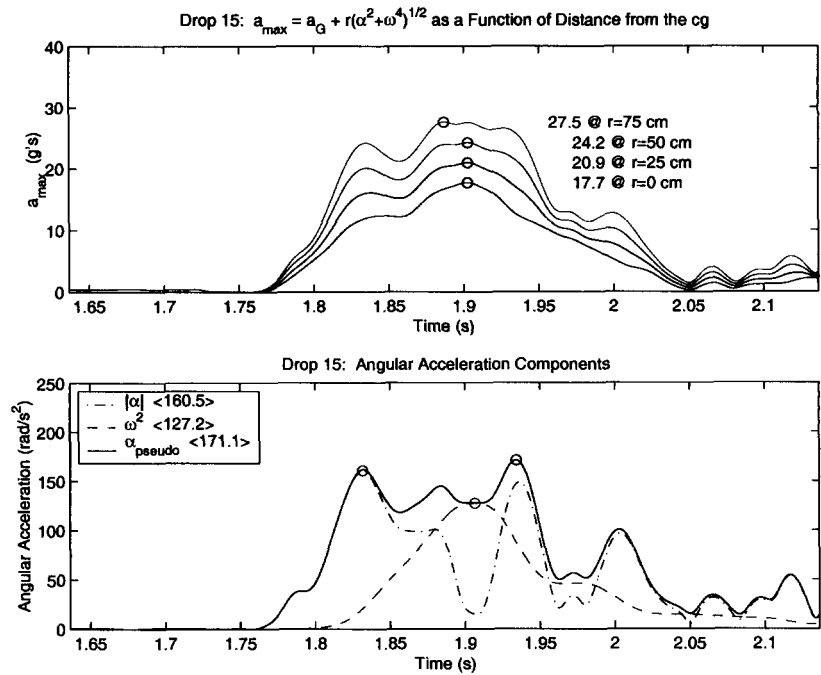


Figure 7: Drop 15 test results from accelerometer analysis.

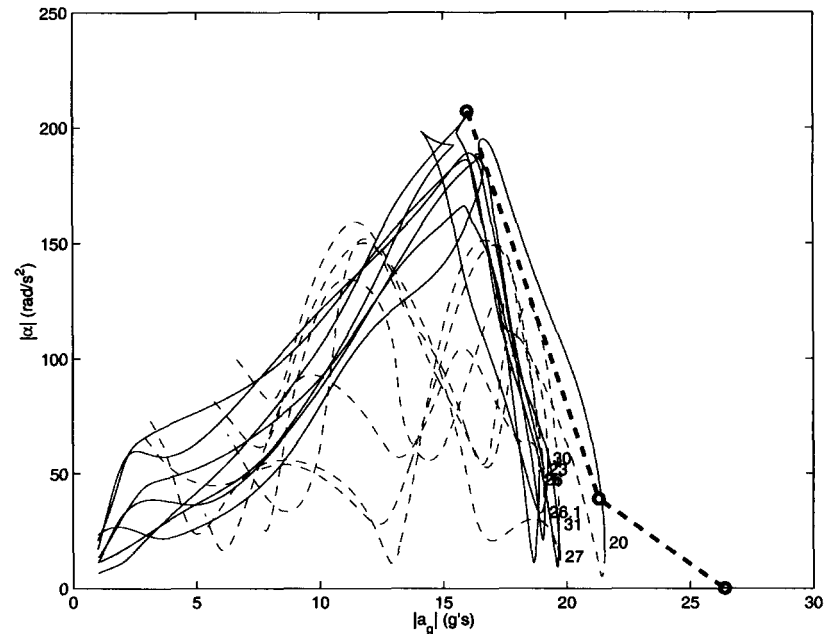


Figure 8. Phase plot of angular acceleration vs. cg acceleration for 60° ramp drops with $11.5 < V_{norm} < 12.5$ m/s (listed in Table 3). Blue solid lines indicate increasing cg acceleration up to the peak value while red dashed lines indicate decreasing cg acceleration. Superimposed in black and connected with a heavy dashed line are the three load events listed in Table 4, which characterize the three loading extremes.

Also, the post-impact cg acceleration DC error was unusually high for Drop 20 indicating that the peak level may be artificially high. This is

Table 4: Summary of loading events used to characterize landing load extremes.

Loading Event	ag (g's)	a (1/s ²)	w (1/s)	Notes:
1	21.3	39.1	13.8	Taken from Drop 14 with LUF=1.15
2	16.0	207.0	10.8	Taken from Drop 13 with LUF=1.15
3	26.4	0.0	13.0	16 m/s superflat with LUF=1.10 & expected ω

supported by the large difference between Drop 20 and the 6 other drops in Fig. 8. Hence, the high level of acceleration for Drop 20 can be considered less reliable and the remaining loads are addressed by the loading events in Table 4. The importance of Drop 20 was further diminished, as it was determined that the dominant loading factor is the linear acceleration, which is maximized in the 26.4 g non-rotating case.

V. Computational Performance Modeling

The MER airbags protect the lander and rover in a manner that is outwardly similar to automotive airbags but that is actually quite different at a functional level. The approach used with automotive airbags is to provide a cushion of air to slow the rate of deceleration using distributed pressure forces applied to the body over some path length. The MER airbags also take advantage of an airbag's stroke but the majority of the load is transferred to the lander in a very different manner that does not rely on the distributed pressure.

The four airbags, illustrated in Fig. 9, are each constructed from six 1.8 m diameter lobes (24 in all) that are held in place and maintain their shape using tendons that capture the membrane forces at the lobe intersections. These tendons are attached to the lander petals at six points on each petal for a total of 24 tendon pin locations. Hence, the airbags are actually held in place on the lander petals rather than the lander being held captive in the interior of the airbags. The upshot of this is that, when the lander and airbags impact the ground, the tendons reacting the pressure forces on the impacting side go slack while the upper tendons remain taut resulting in a net force imbalance on the lander. There will also be an increase in the lower airbag pressure that does contribute to the deceleration, but the majority of the decelerating force is transferred to the lander through the tendon pin attachment points. These internal loads do not affect the sensed accelerations but were the focus of a major effort on MER that is suitable for a separate discussion.

A number of analytical tools were used in an attempt to predict different aspects of the MER landing loads. A program written by ILC Dover as an Excel spreadsheet called Bag-M was used to estimate cg accelerations based on airbag volume loss as a function of lander stroke for a given normal velocity. While the Bag-M model is very simple the results it generated were surprisingly accurate when compared to the drop test data as seen in Table 5.

A more detailed analysis was developed using ADAMS software in an attempt to estimate both the cg acceleration as well as the airbag tendon loads on the MER lander^{1,2,8}. During a landing event the airbag tendon loads shift considerably due to the airbag deformation and lander acceleration. This represented a significant design challenge to the composite lander structure. The four airbags and the lander were each modeled in ADAMS as a total of five rigid bodies connected by elastic elements representing the tendons. The fluid dynamics of the gas in the airbags was modeled using a set of differential equations to estimate the pressure in the airbags and the flow between them^{2,8}. Results for peak acceleration obtained from the ADAMS model are also included in Table 5 for comparison. In addition to the acceleration level, the ADAMS model was also successful at predicting the

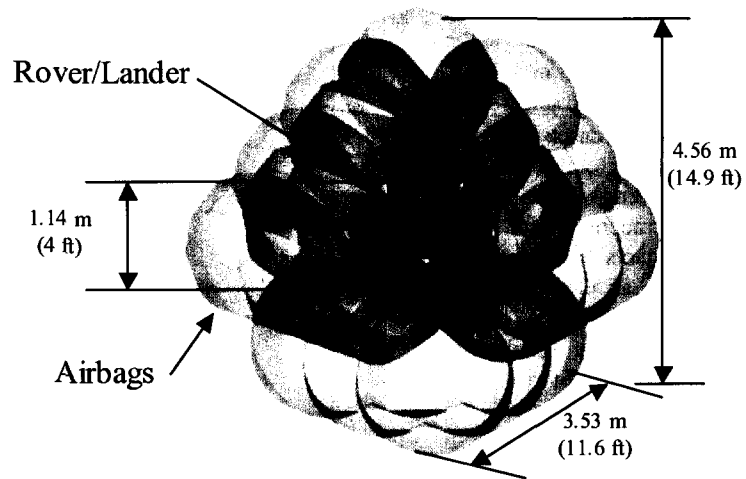


Figure 9: Schematic diagram of the MER lander inside the four airbags.

coefficient of restitution for the lander with an estimate of $e \sim 0.88$ while the test values fell in the range of $0.8 < e < 0.95$ (an amazingly high value for any system, particularly one of this size and mass).

Finally, the internal loads in the lander and rover were estimated using a NASTRAN model and test measured tendon pin data⁷. While this was one of the central purposes the ADAMS model was constructed, it proved to be an elusive and difficult task to model the tendon loads accurately. One clear issue with the ADAMS model is that it uses simple linear elements and rigid bodies to model a nonlinear and deforming impact event. The transfer of loads between different airbags and tendons was captured somewhat but the compliance of the physical system and complexity of the load paths resulted in differences between the measured loads and the model results, although the high load tendon pin locations were accurately identified. Even the loads measured during the tests using load cells were somewhat suspect as different tests under the same conditions often resulted in inconsistent measurements again, due in part, to the shifting of the loads as the airbags interact.

Table 5: Comparison of modeled and measured peak acceleration for a 12 m/s normal impact.

Bag-M	ADAMS	Superflat
(g's)	(g's)	(g's)
16.4	14.7	16.0

VI. Conclusion

The results from a total of 52 airbag drop tests have been analyzed in order to determine the anticipated accelerations and loads for the MER lander. The non-rotating cases were found to represent a lower bound of the cg accelerations and are expected to be typical of secondary impacts having potentially amplified normal velocity components. Analytical tools provide some insight into the cg acceleration but had difficulty predicting the nonlinear airbag tendon pin loads. Finally, the entire dynamic envelope is adequately described by three acceleration cases, which were used to determine the internal lander loads in NASTRAN.

Acknowledgments

The author wishes to acknowledge and to congratulate the MER Entry Descent and Landing team for their hard and diligent work that helped to make the Mars Exploration Rovers a stunning success. The author would also like to thank Chris Landry, Gary Ortiz, Chia-Yen Peng, Tom Rivellini, Dara Sabahi, Moktar Salama, Adam Steltzner, Ben Thoma, Frank Tillman, Walter Tsuha, and Skip Wilson for their contributions to this work during its progress.

References

- ¹Waye, D. E., Cole, J. K., and Rivellini, T. P., "Mars Pathfinder Airbag Impact Attenuation System," 13th AIAA Aerodynamic Decelerator Systems Technology Conference, AIAA-95-1552, Clearwater Beach, FL, May, 1995, pp. 109-119
- ²Salama, M., Davis, G., Kuo, C. P., Rivellini, T., and Sabahi, D., "Simulation of Airbag Impact Dynamics for Mars Landing," AIAA/ASME/AHS Dynamics Specialty Conference, AIAA-96-1209, Salt Lake City, UT, April, 1996
- ³Thoma, B.L., "Mars Exploration Rover Airbag Landing Loads and Analysis," JPL IOM 352D:01:021:BLT, March 26, 2001
- ⁴Thoma, B.L., "MER Airbag Landing Loads and Analysis Update 1," JPL IOM 352D:01:043:BLT, March 26, 2001
- ⁵Adams, D. S., "MER Airbag Landing Loads and Analysis Update 3," JPL IOM 352F:02:033:DSA, December 13, 2002
- ⁶Himmelblau, H., Kern, D. L., Manning, J. E., Piersol, A. G., and Rubin, S., "Dynamic Environmental Criteria," NASA-HDBK-7005, March 13, 2001, pp. 132-134
- ⁷Landry, C. P., "MER Landing Loads Update with Subsequent Bounce Cases," JPL IOM 352F:02:016:CPL, May 20, 2002
- ⁸Tsuha, W. S., and Salama, M. A., "Test/Analysis Correlation for the Mars Pathfinder Lander/Airbag Subsystem: ADAMS Analytical Model," JPL IOM 3542:95:002, January 9, 1995